Sensitivity of *pp* bremsstrahlung on low-energy *NN* interaction

M. D. Cozma, O. Scholten, and R. G. E. Timmermans
KVI, Zernikelaan 25, 9747 AA Groningen, The Netherlands

J. A. Tjon
KVI, Zernikelaan 25, 9747 AA Groningen, The Netherlands
and Department of Physics, University of Maryland, College Park, Maryland 20742-4111, USA
(Received 14 May 2003; published 31 October 2003)

In this paper we investigate possible reasons for the differences found in some kinematic regions between existing microscopic *pp* bremsstrahlung models and experimental data. It is shown that this is partly the result of an inaccurate description of the elastic nucleon-nucleon (*NN*) *T* matrix at low energies. We show that for the phase space probed by the recent KVI experiment, Coulomb corrections do not influence the observables. The difference between theory and experiment is reduced after the *NN* one-boson exchange model is refitted to the *pp* phase shifts, however, a sizable discrepancy persists.

DOI: 10.1103/PhysRevC.68.044003 PACS number(s): 21.45.+v, 13.75.Cs

I. INTRODUCTION

Many years ago, proton-proton bremsstrahlung ($pp\gamma$) was suggested as a tool to discriminate between the various existing two-nucleon potential models [1]. Disagreements between competing theories, the inability of some theoretical treatments to agree with the experiments, as well as the necessity of including contributions previously neglected, has made resolving the resulting confusion about $pp\gamma$ a primary goal.

To describe bremsstrahlung a number of microscopic models have been developed, of which we mention the classical works of Brown [2] and of Heller and Rich [3], and the more recent models of Refs. [4–13]. At present the situation in $pp\gamma$ remains unsatisfactory. The covariant model of Martinus *et al.* [11,12] disagrees with the TRIUMF data [14] for certain asymmetric proton angles. Moreover, the absolute normalization of the TRIUMF data remains controversial. Also for the high-precision KVI data [15] there is a significant discrepancy between theory and experiment for asymmetric proton angles.

The size of the discrepancy is disturbing, since what primarily enters in the computation of the bremsstrahlung amplitude are the *NN* interaction and the electromagnetic coupling of the photon to the nucleon-nucleon (*NN*) system, both of which had been believed to be accurately known. The high precision of the KVI experimental data allows in principle also the study of smaller effects such as, for example, the negative-energy states, the Δ isobar, or the meson-exchange currents. The observed discrepancy seems too large to be due to these effects.

In this paper we investigate possible origins of the discrepancy between the $pp\gamma$ model of Martinus *et al.* [11,12] and the experimental data of KVI. It is shown that it appears for kinematics for which the dominant contribution comes from terms which involve the elastic *T* matrix evaluated at laboratory kinetic energies below about 15 MeV. It is thus inferred that at least an important part of the problem resides in the description of the low-energy *NN* interaction. Since at such low energies the Coulomb interaction becomes important, we also investigate its role in *pp* bremsstrahlung. This is done within a toy model for bremsstrahlung, in which only the *pp* interaction in the $^1S_0$ channel is considered.

The paper is organized as follows. The main ingredients of the Martinus *et al.* model for bremsstrahlung are presented, its predictions are compared with the KVI experimental data, and possible sources of the mentioned discrepancy are investigated in Sec. II. In Sec. III a toy model for bremsstrahlung is developed. Coulomb corrections to the strong interaction are included and the sensitivity of the bremsstrahlung observables on the low-energy *NN* interaction is demonstrated. We then show that the discrepancy between theory and experiment can be partly removed by improving the *NN* potential in the low-energy region (Sec. IV). We end by summarizing our conclusions.

II. A COVARIANT MODEL FOR BREMSSTRAHLUNG AND COMPARISON WITH DATA

A. A relativistic covariant model

In this section, the main ingredients of the Martinus *et al.* model [11,12] for bremsstrahlung are summarized. In relativistic field theories the *T* matrix for the scattering of two nucleons is a solution of the inhomogeneous Bethe-Salpeter (BS) equation

$$T(p,p';P) = V(p,p') - i\int \frac{d^4k}{(2\pi)^4} V(p,k) S_2(k,P) T(k,p';P), \tag{1}$$

where $S_2(p,P)$ is the free two-body propagator which is given by the direct product of two one-particle, free-fermion propagators with relative momentum p and total momentum P. The *NN*-interaction kernel is chosen to be given by the one-boson exchange model of Fleischer and Tjon [16]. In this one-boson exchange (OBE) model the strong interaction is described by the exchange of a few

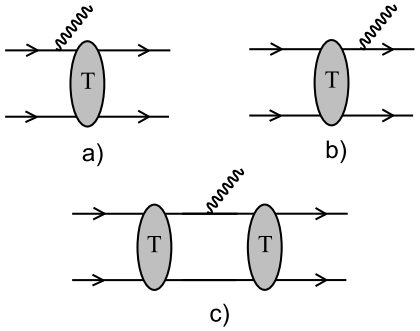

FIG. 1. Single-scattering diagrams contributing to the impulse approximation [(a) and (b)] and the rescattering diagram contribution (c). Diagrams in which the photon couples to only one of the protons are shown.

mesons: π, ρ, δ, η, ω, and ϵ (or σ). The tree-level OBE potential is presented in Appendix A.

Within the OBE model the full BS equation can in principle be solved. In practice, this is a highly nontrivial task due to the four-dimensional integrals, which need to be computed in a space with an indefinite metric and due to the pole structure of the propagators. Therefore, a quasipotential approximation is usually made. This consists in replacing the two-particle propagator by one in which the relative energy is restricted, but properties such as two-particle unitarity and relativistic covariance are maintained. One such possible choice, which will be used in the following, due to Blankenbecler-Sugar-Logunov-Tavkhelidze [17] (known as BSLT or equal-time approximation), consists of replacing the scalar part of the two-nucleon propagator,

$$G_0 = \frac{1}{\left(\frac{1}{2}P+p\right)^2 - M^2 + i\epsilon}\frac{1}{\left(\frac{1}{2}P-p\right)^2 - M^2 + i\epsilon} \tag{2}$$

by

$$G_2^{BSLT} = i\pi\frac{1}{E_p - E}\frac{1}{(E_p+E)^2}\delta(p_0). \tag{3}$$

The two-particle propagator becomes

$$S_2^{BSLT}(p,P) = \frac{1}{2}(E_p - E)\,\delta(p_0)S^{(1)}(p,P)S^{(2)}(p,P), \tag{4}$$

where $E=\frac{1}{2}P_0$ and $E_p=\sqrt{p^2+M^2}$. Using the above form of the propagator the integration over the relative energy can be performed in the BS equation. One is left with the BSLT equation, which can be handled more easily from a practical point of view,

$$T(\hat{p},\hat{p}';P) = V(\hat{p},\hat{p}') - i\int\frac{d^4k}{(2\pi)^4}V(\hat{p},\hat{k})S_2^{BSLT}(\hat{k},P)T(\hat{k},\hat{p}';P), \tag{5}$$

where the four-momentum $\hat{k}$ is restricted by the δ function in S_2 such that in the center-of-mass frame of the two nucleons its time component is zero, i.e., $\hat{k}_0=0$.

The BSLT equation can be solved in a partial-wave basis [18]. The partial-wave decomposition yields a system of coupled one-dimensional equations for the partial-wave amplitudes. The equation is solved keeping also the contributions from negative-energy states both as intermediate states or initial (final) states. The latter case is relevant only when one considers the half or the fully off-shell T matrix. The on-shell T matrix was fitted to the *np* phase shifts of Arndt *et al.* [19] by varying the meson-nucleon coupling constants. The OBE model presented here has been successfully applied to the case of electron-deuteron scattering [18].

The electromagnetic nuclear current can be split into two parts: the one-body and the two-body current, the former giving the dominant contribution in the energy region we are considering. The invariant amplitude of the bremsstrahlung process is $M_{fi}=\epsilon^\mu\langle f|J_\mu|i\rangle$, with ϵ^μ the polarization four-vector of the emitted photon, while J_μ is the nuclear current, which has its matrix elements given by

$$\left\langle f\left|J_\mu\right|i\right\rangle = \left\langle p',P'\left|T(p',\tilde{p};P')S^{(1)}(\tilde{p},P')\Gamma_\mu^{(1)}(q)\right|p,P\right\rangle + \left\langle p',P'\left|\Gamma_\mu^{(1)}(q)S^{(1)}(\tilde{p}',P)T(\tilde{p}',p;P)\right|p,P\right\rangle + (1\leftrightarrow 2) - i\int\frac{d^4k}{(2\pi)^4}\langle p',P'|T(p',k';P')S^{(1)}(k',P')\Gamma_\mu^{(1)}(q)S_2(k,P)T(k,p;P)|p,P\rangle. \tag{6}$$

The first two terms correspond to what is commonly known as the impulse approximation (IA). These terms correspond to the sum of all single-scattering diagrams, when the photon is emitted by one of the external legs. Consistency with the equal-time approximation imposes that the dependence of the elastic T matrix on the off-shell energy of the particle from which the photon is emitted is neglected. This amounts to omitting the retardation effects. It was shown by Martinus *et al.* [12] that this introduces uncertainties of at most 10% at 280 MeV. For the case of the KVI

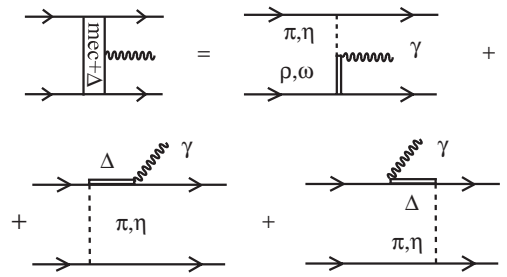

FIG. 2. The Born terms of the two-body current bremsstrahlung. The first one is a MEC contribution, the other two are contributions of the Δ isobar.

experiment at 190 MeV, the effects are even smaller. In more detail, the expression for one of the IA contributions (final-state emission from leg 1) is

$$\langle f|J_\mu^{(IA)}|i\rangle = \langle p_1', p_2'|\Gamma_\mu^{(1)}(q)S^{(1)}(p_1'+q) \times T(\hat{p}_1'+\hat{q}, \hat{p}_2'; p_1, p_2)|p_1, p_2\rangle, \quad (7)$$

where the hat over some momenta labeling the elastic T matrix means that in the center of mass of the nucleons their zeroth component will be set equal to zero.

The last term in Eq. (6) is the rescattering contribution to bremsstrahlung (see Fig. 1). The four-dimensional integral appearing here is easily reduced to a three-dimensional one [11,12] since, as a result of the equal-time approximation, the elastic T matrix appearing in the integrand does not depend on the relative energy of the two nucleons, k_0. The k_0 integral for the rescattering diagram (the photon being emitted by the particle labeled i) is then of the form

$$I_0^{(i)} = \int \frac{dk_0}{2\pi} S^{(i)}(k_0, \vec{k}-\vec{q}; E')\Gamma_\mu^{(i)}(q)S_2(k_0, \vec{k}; E), \quad (8)$$

with $(\omega, \vec{q})$ the photon four-momentum, and can easily be evaluated analytically; $S_2(k_0, \vec{k}; E)$ is the two-particle free propagator. This is consistent with the equal-time framework used for treating the elastic *NN* problem.

In addition, contributions from the two-body currents, depicted in Fig. 2, have been considered. They include contributions from the meson-exchange currents (MEC) and the Δ isobar. Details are presented in Appendix B.

For the case of *pp* bremsstrahlung the $NN\gamma$ vertex is taken to be

$$\Gamma_\mu^{(i)}(q) = e\left(\gamma_\mu^{(i)} - \frac{i\kappa}{2M}\sigma_{\mu\nu}^{(i)}q^\nu\right), \quad (9)$$

where e is the proton electric charge and $\kappa=1.79$ is the anomalous magnetic moment of the proton. Within the present model, *NN* partial waves of angular momentum up to and including $J=9$ have been considered. This is the case for all figures if not otherwise stated. In our analysis it was convenient to sometimes restrict the model to partial waves up to and including $J=2$, which is being mentioned at the pertinent places.

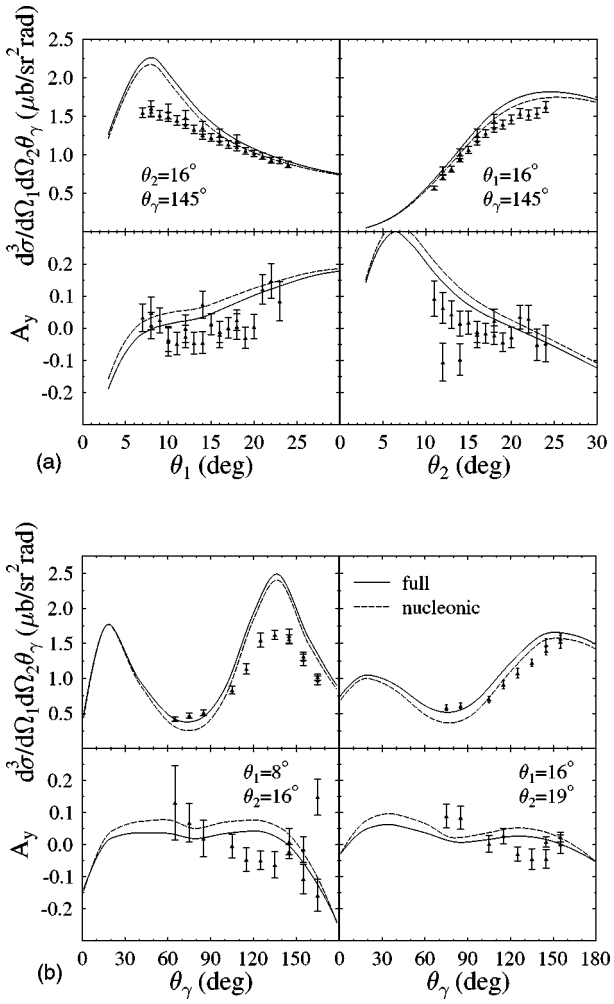

FIG. 3. Bremsstrahlung cross sections and analyzing powers at T_{lab}=190 MeV incoming proton kinetic energy for several kinematics. In the left panel θ_2=16°,θ_γ=145° and θ_1=16°,θ_γ=145° as a function of the remaining outgoing proton angle; in the right panel θ_1=8°,θ_2=16° and θ_1=16°,θ_2=19° as a function of the photon angle θ_γ. Predictions of the Martinus *et al.* model are compared with data of the KVI experiment. The dashed line includes contributions only from the nucleonic current, while for the full line MEC and the Δ isobar contributions were also taken into account.

B. Comparison with data

In Fig. 3 we have plotted the bremsstrahlung predictions of the relativistic model for a few kinematical regions, as a function of the angle of the emitted photon (θ_γ) or of one the outgoing protons. The polar angles of the outgoing protons are denoted by θ_1 and θ_2, the emitted photon being on the same side of the incident beam as the outgoing proton 1. For comparison, the experimental results of the KVI experiment [15], performed at a proton energy of 190 MeV, are plotted. For two of the kinematics plotted here (namely, θ_2=16°,θ_γ=145° and θ_1=8°,θ_2=16°), a large discrepancy between theory and experiment is observed [20]. In both cases the discrepancy appears at angles where the cross section has a peak. The same type of discrepancy is present also for other kinematics of the KVI experiment, which are not presented here. Still, for a number of kinematical regions theory and

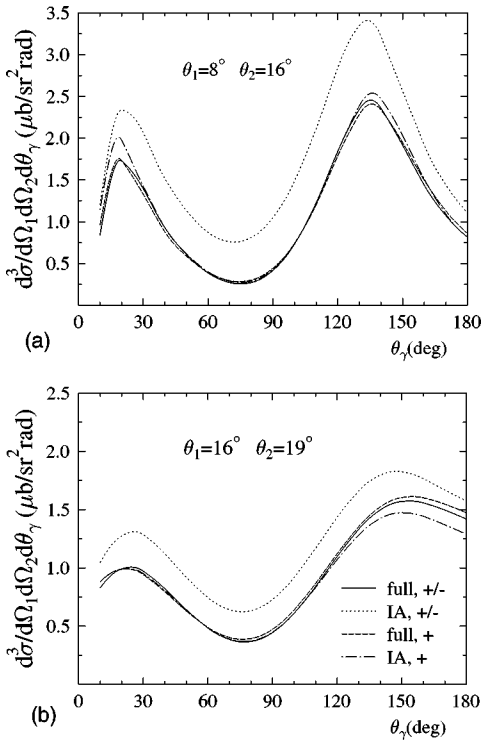

FIG. 4. The effect of the negative-energy states on the bremsstrahlung cross section is illustrated for two kinematics at T_{lab} =190 MeV for θ_1=8°,θ_2=16° and θ_1=16°,θ_2=19°. Calculations including both the negative- and positive-energy states (+/−) or only the positive-energy states (+) are shown. Results for the impulse approximation (IA) and the full nucleonic (IA+rescattering) contributions are shown. It is seen that the full calculation with only positive-energy states included is close to the full calculation with both positive- and negative-energy states included, in agreement with the soft-photon theorem for bremsstrahlung.

experimental data are in reasonable agreement. Two such cases are presented here: θ_1=16°,θ_γ=145° and θ_1=16°,θ_2 =19°. The size of the discrepancy is disturbing, since the ingredients that go into the computation of the bremsstrahlung amplitude (*NN* interaction, $NN\gamma$ vertex) are thought to be well understood and described.

As already mentioned, various contributions have been considered in the Martinus *et al.* model for bremsstrahlung: nucleonic (impulse approximation and rescattering diagrams), MEC and Δ-isobar contributions. We note that it is unlikely that the discrepancy is due to a poor description of the MEC and Δ-isobar terms, since their contributions for the kinematics studied here is small, especially at the position of the cross-section peaks (see Fig. 3). We will thus concentrate on the nucleonic contribution. The contribution of the rescattering diagram is important (Fig. 4), giving a sizable decrease of the cross section, with respect to the IA result, when both the positive- and negative-energy states are considered. The main part of its contribution comes from coupling to the negative-energy states, the positive-energy state contribution is modest (compare the dashed and the dash-dotted curves). Negative-energy state contributions from the IA diagrams and from the rescattering diagram cancel each other to a large extent as can be seen from Fig. 3. This has been shown to hold up to photon energies of about 100 MeV [12]. The cancellation becomes exact in the limit of photon energy going to zero, as required by the soft-photon theorem for bremsstrahlung [21]. Keeping only the positive-energy states is thus a good approximation to the full nucleonic result. We conclude that the mentioned discrepancy already resides at the level of IA diagrams. For the IA diagrams, we have determined contributions of the different partial waves separately. This allows us to understand the difference between kinematical regions like θ_1=8°,θ_2=16° and θ_1 =16°,θ_2=19° in order to discover the possible source of these discrepancies. The results for the first few *NN* partial waves contributing to $pp\gamma$, at the region of the cross-section peaks, are shown in Table I. From this table it is clear that for the specific kinematics we have chosen, only a few partial waves are important for bremsstrahlung: $^1S_0$, $^3P_1$, and $^3P_2$.

A further insight is obtained once the kinematics of the four cases are analyzed. There are two distinct energy values at which the elastic *T* matrix is evaluated: one is the kinetic

TABLE I. Cross sections, in μb/sr^2 rad, for different kinematics $\theta_1,\theta_2,\theta_\gamma$, split up in partial waves, radiation from initial and final proton legs, and the total; only contributions from the positive-energy states have been considered. The results of the last four rows of the table are obtained by considering all the partial waves up to J=2 together. The kinematics correspond to the backward peak in the cross section. Similar results are found for different values of θ_γ, while keeping θ_1 and θ_2 fixed.

	θ_1, θ_2, θ_γ					
	8°, 16°, 139.5°			16°, 19°, 159.3°		
	Initial	Final	Total	Initial	Final	Total
$^1S_0$	1.802	0.001	1.805	0.441	0.001	0.444
$^3P_0$	0.012	0.000	0.013	0.006	0.000	0.006
$^3P_1$	0.049	0.093	0.125	0.061	0.122	0.186
$^3P_2$	0.159	0.254	0.427	0.192	0.374	0.567
$^1D_2$	0.000	0.002	0.003	0.001	0.000	0.002
Initial		2.165			0.889	
Final		0.456			0.730	
External legs		2.507			1.556	
External legs+rescattering		2.372			1.721	

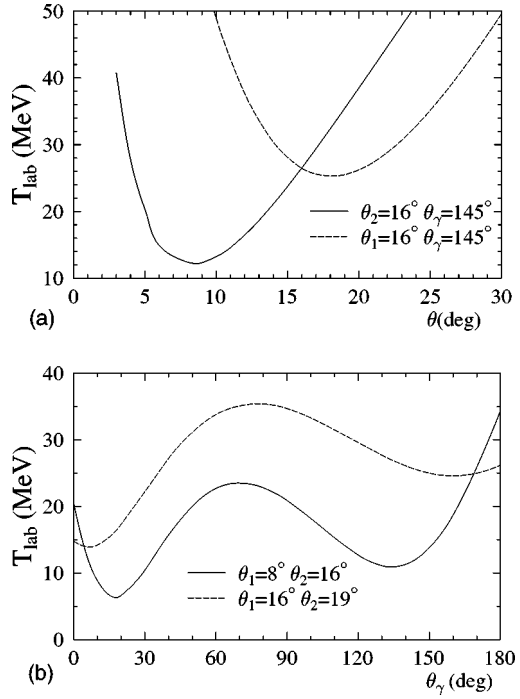

FIG. 5. Kinetic energy of the incoming proton at which the elastic *NN T* matrix is evaluated in the case of initial state bremsstrahlung, for the kinematics discussed in the text. For the case of final-state bremsstrahlung the *T* matrix is evaluated at 190 MeV.

energy of the projectile proton (in the case of the final-state bremsstrahlung), and the other one is the kinetic energy of the outgoing proton (initial-state bremsstrahlung). The latter can be very low, since the emitted photons are energetic. For the rescattering diagram, both cases occur, since the elastic *T* matrix is evaluated at high energy before emission and at low energy after emission. In Fig. 5, the energy $(T_{lab}=[(E_1'+E_2')^2-(\vec{p}_1+\vec{p}_2)^2]/2M-2M)$ at which the elastic *NN T* matrix is evaluated is plotted as a function of the unspecified proton angle (θ_1 or θ_2) (left panel), and as a function of the photon angle (right panel). The two panels correspond to the kinematics presented in Fig. 3. It is seen that the kinematical points in disagreement with the experiment correspond to those for which the elastic *T* matrix is evaluated at low energies (of the order of 10 MeV). The lowest energies correspond to the cross-section peaks. For the $\theta_1=16°, \theta_\gamma=145°$ and $\theta_1=16°$, $\theta_2=19°$ cases the elastic *T* matrix is evaluated at energies above 25 MeV.

In Fig. 6 we have plotted the difference between the theoretical and experimental values of the differential cross section as a function of the kinetic energy of the outgoing protons T_{lab} for the four kinematical cases presented here. It supports the previous conclusion that there is a systematic large discrepancy between the theory and experiment for the cases for which the energy of the outgoing proton system is less than 15 MeV. A similar figure, with data points for other kinematical regions, has been presented in Ref. [22]. An increase of the discrepancy with the decrease of the kinetic energy T_{rel} is seen.

The above considerations lead us to the conclusion that a significant discrepancy is present for the kinematics for

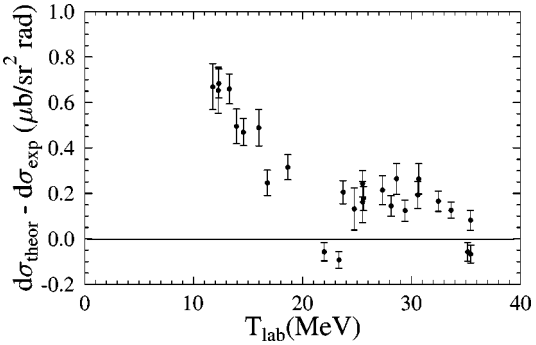

FIG. 6. The difference between the theoretical predictions of the covariant bremsstrahlung model and the experimental results of the KVI experiment, shown as a function of the kinetic energy of the outgoing protons (in a frame in which one of the protons is at rest).

which the final *pp* system has a low kinetic energy. We note that in both the single-scattering diagrams and the rescattering diagram the elastic *T* matrix enters, evaluated at this low energy. It is thus plausible that part of the problem resides in a poor description of the elastic *T* matrix at low energies, and since at low energies most of the interaction goes via the $^1S_0$ channel, we conclude that this partial wave is at the origin of most of the observed discrepancy [20]. For both cases presented in Table I, ^3P waves are important: for the $\theta_2=16°, \theta_\gamma=145°$ case they are somewhat less important than the $^1S_0$ partial wave, while for the $\theta_1=16°, \theta_\gamma=145°$ kinematics their contribution is dominant. Important contributions of the ^3P waves arise in diagrams in which the elastic *T* matrix is evaluated at high energies. For an accurate description of bremsstrahlung, it is thus necessary that the ^3P waves are accurately reproduced by the OBE model we use at an energy equal to that of the incoming proton. But, since kinematics dominated by ^3P waves are in good agreement with the experiment (suggesting a reasonable description of these partial waves), we will concentrate on the $^1S_0$ partial-wave contributions to the *NN* potential.

An additional concern comes from the fact that since we are dealing with charged particles, Coulomb corrections have to be accounted for. A complete treatment of the Coulomb interaction within the framework of a nonrelativistic potential model is given in the classical paper of Heller and Rich [3]. The cross section for pure Coulomb bremsstrahlung has been shown to be small (of the order of nanobarns), and thus it will be of no practical importance to consider it. However, the Coulomb corrections to the strong bremsstrahlung amplitude might be important. Including them in a relativistic model is difficult due to the long-range nature of the Coulomb interaction. We will study their effect on the $pp\gamma$ cross section within a toy model, which is the topic of the following section.

III. TOY MODEL OF BREMSSTRAHLUNG

To investigate the effect of the Coulomb force, a simple nonrelativistic model for bremsstrahlung is developed. The *NN* interaction will be treated using a simple separable potential. Only contributions from the $^1S_0$ partial wave are con-

sidered here. The bremsstrahlung amplitude is computed by evaluating the matrix elements of the electromagnetic current between incoming and outgoing Coulomb waves. For clarity, we will start by summarizing some of the conventions used.

The full Hamiltonian of our problem is given by

$$H = H_0 + V_C + V_S, \tag{10}$$

with H_0 being the free-particle Hamiltonian, while V_C and V_S are the Coulomb and the strong potential, respectively. The eigenvalue problems, in a concise notation, for the free particle, a particle in a Coulomb potential and a particle in a Coulomb + strong potential are given, respectively, by

$$H_0|\vec{p}\rangle = E_0|\vec{p}\rangle, \tag{11}$$

$$(H_0 + V_C)|\psi_{\vec{p}}\rangle = E_C|\psi_{\vec{p}}\rangle,$$

$$(H_0 + V_C + V_S)|\phi_{\vec{p}}\rangle = E_{SC}|\phi_{\vec{p}}\rangle.$$

Starting from the Schrödinger equation one can also introduce the Green's functions (propagators) with appropriate boundary conditions. We will make use of the retarded and advanced propagators, denoted by $G^{(+)}$ and $G^{(-)}$, with appropriate subscripts: $_0$ for the free propagator, C for the Coulomb modified propagator and SC for the total propagator,

$$G^{(\pm)}(E) = \frac{1}{E - H \pm i\varepsilon}. \tag{12}$$

The relations between the energy states introduced in Eq. (11) are

$$|\psi_{\vec{p}}^{(\pm)}\rangle = [1 + G_C^{(\pm)}V_C]|\vec{p}\rangle, \tag{13}$$

$$|\phi_{\vec{p}}^{(\pm)}\rangle = [1 + G_{SC}^{(\pm)}(V_C + V_S)]|\vec{p}\rangle, \tag{14}$$

$$|\phi_{\vec{p}}^{(\pm)}\rangle = [1 + \sum_{n=1}^{\infty}(G_C^{(\pm)}V_S)^n]|\psi_{\vec{p}}^{(\pm)}\rangle. \tag{15}$$

A. The two-potential formalism

The two-potential formalism was developed [23,24] to deal with situations when physical processes are influenced by two interactions (potentials) and one of them needs to be treated nonperturbatively, while for the other one a perturbative expansion suffices. Such a case is met in practice when the strong interaction is studied in regions of the phase space where the Coulomb interaction is known to be of some relevance.

Starting from the S matrix

$$S_{fi} = \langle\phi_{\vec{p}'}^{(-)}|\phi_{\vec{p}}^{(+)}\rangle \tag{16}$$

and using the Lippmann-Schwinger equation for the full wave function

$$\phi_{\vec{p}}^{(\pm)} = \psi_{\vec{p}}^{(\pm)} + G_C^{(\pm)}V_S\phi_{\vec{p}}^{(\pm)}, \tag{17}$$

or its formal solution

$$\phi_{\vec{p}}^{(\pm)} = \psi_{\vec{p}}^{(\pm)} + G^{(\pm)}V_S\psi_{\vec{p}}^{(\pm)}, \tag{18}$$

it is straightforward to arrive at

$$S_{fi} = \langle\psi_{\vec{p}'}^{(-)}|\psi_{\vec{p}}^{(+)}\rangle + \langle\psi_{\vec{p}'}^{(-)}|G_C^{(+)}(E_{\vec{p}})V_S|\phi_{\vec{p}}^{(+)}\rangle + \langle\psi_{\vec{p}'}^{(-)}|V_S G^{(+)}(E_{\vec{p}'})|\phi_{\vec{p}}^{(+)}\rangle. \tag{19}$$

One then makes use of the fact that the Coulomb waves and the full waves are eigenvectors of, respectively, the Coulomb and the full propagator,

$$\begin{aligned} S_{fi} &= \left\langle \psi_{\vec{p}'}^{(-)}|\psi_{\vec{p}}^{(+)}\right\rangle + \frac{1}{E_p - E_{p'} + i\varepsilon}\left\langle \psi_{\vec{p}'}^{(-)}\right| V_S|\phi_{\vec{p}}^{(+)}\rangle \\ &\quad + \frac{1}{E_{p'} - E_p + i\varepsilon}\langle\psi_{\vec{p}'}^{(-)}|V_S|\phi_{\vec{p}}^{(+)}\rangle \\ &= \langle\psi_{\vec{p}'}^{(-)}|\psi_{\vec{p}}^{(+)}\rangle - 2i\pi\delta(E_{p'} - E_p)\langle\psi_{\vec{p}'}^{(-)}|V_S|\phi_{\vec{p}}^{(+)}\rangle \\ &= \langle\psi_{\vec{p}'}^{(-)}|\psi_{\vec{p}}^{(+)}\rangle - 2i\pi\delta(E_{p'} - E_p)\langle\phi_{\vec{p}'}^{(-)}|V_S|\psi_{\vec{p}}^{(+)}\rangle. \end{aligned} \tag{20}$$

The equivalent expression for the T matrix reads

$$\begin{aligned} T_{fi} &= \langle\vec{p}'|V_C|\psi_{\vec{p}}^{(+)}\rangle + \langle\psi_{\vec{p}'}^{(-)}|V_S|\phi_{\vec{p}}^{(+)}\rangle \\ &= \langle\vec{p}'|V_C|\psi_{\vec{p}}^{(+)}\rangle + \langle\phi_{\vec{p}'}^{(-)}|V_S|\psi_{\vec{p}}^{(+)}\rangle = T_{\vec{p}',\vec{p}}^{C} + T_{\vec{p}',\vec{p}}^{SC}. \end{aligned} \tag{21}$$

We will apply this formalism to the $pp\gamma$ process. The derivation in this section is general and for the moment we will adopt a simple expression for the electromagnetic operator (ignoring the magnetic moment of the proton) and will suppress writing frame transformations explicitly. The purpose is to split the bremsstrahlung amplitude in a few terms which will be easier to understand from a diagrammatical point of view. We will consider the following Hamiltonian for the emission (or absorption) of photons,

$$H_{em} = \frac{q}{m}\vec{A}\cdot\vec{P}. \tag{22}$$

The starting point is the expression for the T matrix element for bremsstrahlung [23,25],

$$T(\vec{p}', \vec{p}) = \langle\phi_{\vec{p}'}^{(-)}|H_{em}(1) + H_{em}(2)|\phi_{\vec{p}}^{(+)}\rangle, \tag{23}$$

since both protons can radiate. One can make use of Eq. (15) to express the total wave function in terms of the Coulomb wave function. The bremsstrahlung amplitude is seen to split into three pieces. These are, respectively,

(1) Pure Coulomb bremsstrahlung. This would give the full amplitude if the strong interaction would be turned off,

$$T_{Coul} = \langle \psi^{(-)}_{\vec{p}'} | H_{em} | \psi^{(+)}_{\vec{p}} \rangle = \int d\vec{p}'' \langle \psi^{(-)}_{\vec{p}'} | \psi^{(+)}_{\vec{p}''} \rangle \langle \psi^{(+)}_{\vec{p}''} | H_{em} | \psi^{(+)}_{\vec{p}} \rangle . \tag{24}$$

It is of small importance, as has been shown by various authors and we will not consider it in the actual computation. Here $S(\vec{p}', \vec{p})^C = \langle \psi^{(-)}_{\vec{p}'} | \psi^{(+)}_{\vec{p}} \rangle$ is the pure Coulomb elastic S matrix.

(2) External-legs bremsstrahlung. There are two contributions of this type: initial-state bremsstrahlung, i.e., the photon is first emitted and then the interaction between the two protons takes place, and final-state bremsstrahlung. The expressions for these processes are given by

$$T^{(i)}_{SC} = \langle \phi^{(-)}_{\vec{p}'} | V_S G^{(+)}_C(E_f) H_{em} | \psi^{(+)}_{\vec{p}} \rangle = \int d\vec{p}'' \langle \phi^{(-)}_{\vec{p}'} | V_S | \psi^{(+)}_{\vec{p}''} \rangle \langle \psi^{(+)}_{\vec{p}''} | G^{(+)}_C(E_f) H_{em} | \psi^{(+)}_{\vec{p}} \rangle, \tag{25}$$

and

$$T^{(f)}_{SC} = \langle \psi^{(-)}_{\vec{p}'} | H_{em} G^{(+)}_C(E_i) V_S | \phi^{(+)}_{\vec{p}} \rangle = \int d\vec{p}'' \langle \psi^{(-)}_{\vec{p}'} | H_{em} G^{(+)}_C(E_i) | \psi^{(-)}_{\vec{p}''} \rangle \langle \psi^{(-)}_{\vec{p}''} | V_S | \phi^{(+)}_{\vec{p}} \rangle, \tag{26}$$

$T(\vec{p}', \vec{p})^{SC} = \langle \psi^{(-)}_{\vec{p}'} | V_S | \phi^{(+)}_{\vec{p}} \rangle$ being the elastic Coulomb-corrected strong T matrix, as given by the two-potential formalism.

Rescattering contribution

$$T^{(resc)}_{SC} = \langle \phi^{(-)}_{\vec{p}'} | V_S G^{(+)}_C(E_f) H_{em} G^{(+)}_C(E_i) V_S | \phi^{(+)}_{\vec{p}} \rangle = \int d\vec{p}'' d\vec{p}''' \langle \phi^{(-)}_{\vec{p}'} | V_S | \psi^{(+)}_{\vec{p}''} \rangle \times \langle \psi^{(+)}_{\vec{p}''} | G^{(+)}_C(E_f) H_{em} G^{(+)}_C(E_i) | \psi^{(-)}_{\vec{p}'''} \rangle \langle \psi^{(-)}_{\vec{p}'''} | V_S | \phi_{\vec{p}} \rangle . \tag{27}$$

This term is not considered any further in the present calculation, since its contribution is expected to be very small due to the fact that the *NN* potential only acts in the $^1S_0$ channel.

B. Elastic *pp* scattering with a separable potential

Separable potentials have been used in the past as a simple approximation to the *NN* potential [26,27]. Such an approximation is suitable for regions near a bound-state pole [28]. Since the $^1S_0$ interaction has such a pole near $E=0$, the separable interaction in this partial wave is a good approximation. The potential is taken to be of the form

$$V(p', p) = \lambda g(p') g(p). \tag{28}$$

Depending on the explicit expression of $g(p)$, there can be additional parameters besides the coupling constant λ. They can be determined by fitting the scattering amplitude to the effective-range expansion, i.e., the scattering length a and the effective range r_e. For the *np* system the standard effective-range formula for the case $\alpha=0$ has to be reproduced, while in the case of the *pp* system the modified effective-range formula is used, i.e.,

$$p(\cot\,\delta - i) = -\frac{1}{2\pi^2 m} \frac{e^{2i\sigma_0}}{T_{SC}(p)}, \tag{29}$$

$$C^2_\eta p(\cot\,\delta - i) + \alpha m H(\eta) = -\frac{1}{a_C} + \frac{1}{2} r_0 p^2,$$

with

$$C^2_\eta = \frac{2\pi\eta}{e^{2\pi\eta} - 1}, \quad \eta = \frac{\alpha m}{2p}. \tag{30}$$

The conventional effective-range formula is obtained by taking the limit $\alpha \to 0$ in Eq. (29) above.

In the absence of Coulomb interaction ($\alpha=0$), the elastic T matrix is obtained by summing the perturbative series expansion, which is of the form of a geometric series,

$$T_{\vec{p}', \vec{p}} = \sum_{n=0}^{\infty} \left\langle \vec{p}' \middle| V_S [G^{(+)}_0(E) V_S]^n \middle| \vec{p} \right\rangle = \frac{\lambda g(p') g(p)}{1 - \lambda I_0(p)}, \tag{31}$$

with the loop integral given by

$$I_0(p) = \int d^3\vec{k}\, g(k)^2 \frac{m}{p^2 - k^2 + i\varepsilon}. \tag{32}$$

The form factor $g(p)$ is chosen such that the loop integral is convergent.

When the Coulomb interaction is added, the potential remains separable. One can treat the problem as if only one potential was present, separable, with the matrix elements between plane waves given by $V(p', p) = \lambda g_c(p') g_c(p)$. In order to derive an expression for $g_c(p)$, one starts from the expression of the Coulomb-corrected T matrix,

$$T^{SC}_{\vec{p}', \vec{p}} = \sum_{n=0}^{\infty} \langle \psi^{(-)}_{\vec{p}'} | V_S [G^{(+)}_C(p^2/m) V_S]^n | \psi^{(+)}_{\vec{p}} \rangle. \tag{33}$$

By inserting a complete set of states at various places one can easily derive that the Coulomb-corrected T matrix can be written in the form

$$T^{(SC)}_{\vec{p}', \vec{p}} = \frac{\lambda g_c(p') g_c(p) e^{i\sigma_0(p') + i\sigma_0(p)}}{1 - \lambda I(p)}, \tag{34}$$

$$I(p) = \int d^3\vec{k}\, g_c(k)^2 \frac{m}{p^2 - k^2 + i\varepsilon},$$

with $g_c(p)$ given by

$$g_c(p) = \int d^3\vec{k}\, g(k) \langle \psi_{\vec{p}} | \vec{k} \rangle, \tag{35}$$

where $\langle \psi_{\vec{p}} | \vec{k} \rangle$ is the Coulomb wave function in the momentum representation. For $\alpha=0$ it reduces to $\delta^3(\vec{p} - \vec{k})$ and thus $g_c(p) = g(p)$, as it should be. For the particular case of

an *S*-wave potential the expression of g_c can be shown to be

$$g_c(p) = \frac{2}{\pi p}\int_0^\infty dr\ rF_0(pr)\int_0^\infty dq q^2 g(q) j_0(qr). \quad (36)$$

Here $F_0(pr)$ is the regular Coulomb wave function for $l=0$, while $j_0(qr)$ is the spherical Bessel function. Using this relation one can in principle determine g_c and then use it to determine the Coulomb-corrected elastic T matrix.

In the following calculations a specific choice for the $g(p)$ form factor has been made,

$$g(p) = \frac{1}{p^2+\beta^2}, \quad (37)$$

which will reproduce the effective-range formula expression, plus a term proportional to p^4. In this particular case an analytical expression for the couplings, in terms of the strong scattering length and effective range, can be obtained,

$$\lambda = \frac{2\beta^3}{\pi^2 m(1-r_e\beta)}, \quad (38)$$

$$\beta = \frac{3}{2r_e}\left(1+\sqrt{1-\frac{16r_e}{9a}}\right).$$

Also the Coulomb-corrected form factor g_c can be obtained analytically [29],

$$g_c(p) = \frac{1}{p^2+\beta^2} C_{\eta(p)} e^{2\eta \arctan(p/\beta)}, \quad (39)$$

but the loop integral which appears in the expression of the elastic T matrix has to be evaluated numerically. The T matrix has been fitted to reproduce the experimental $^1S_0$ phase shifts of both a *np* and a *pp* potential. The results are plotted in Fig. 7, where plots of a *np*+Coulomb and a *pp* without Coulomb system are also plotted to show the effect of the Coulomb interaction on the phase shifts. Since in the computation of bremsstrahlung the T matrix at an off-shell point is needed, we have plotted in Fig. 8 both the real and the imaginary part of the elastic T matrix for the *pp* potential and have shown which are the effects of Coulomb interaction on them. In the region needed for the KVI bremsstrahlung experiment, namely high off-shell momenta, the influence of Coulomb interaction is small. The difference between our computation and the one of Ref. [29] lies in the real part of the loop integral: we compute its exact value numerically, while in Ref. [29] only an approximate, though rather accurate (there, only the first term of the power expansion in α was kept) expression is derived.

C. Bremsstrahlung

To compute the bremsstrahlung amplitude only the contributions from the external legs were kept,

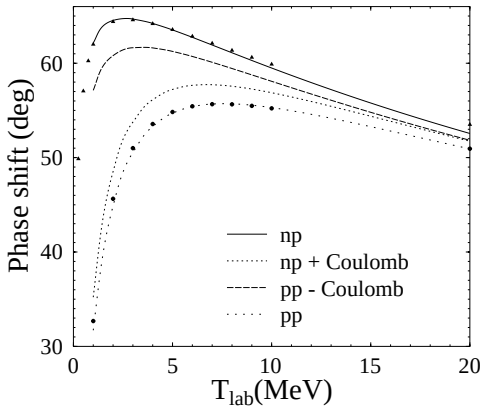

FIG. 7. Phase shifts for the separable potential with $g(p)=1/(p^2+\beta^2)$ for *pp* and *np* scattering (both in the absence and presence of the Coulomb interaction). For the *np* system $a=-23.7$ fm and $r_e=2.62$ fm, while for the *pp* system $a=-7.79$ fm and $r_e=2.48$ fm; when the Coulomb interaction is switched off, for the *pp* system, these parameters become $a^{(s)}=-18.1$ fm and $r_e^{(s)}=2.60$ fm. For comparison, also the phase shifts for the *np* (triangles) and *pp* (circles) cases as given by the PWA93 analysis are shown.

$$S_{SC}^{(ini)} = m\int d\vec{p}'' T^{SC}_{\vec{p}',\vec{p}''} \frac{1}{\vec{p}'^2 - \vec{p}''^2 + i\varepsilon} \langle \psi^{(+)}_{\vec{p}''} | H_{em} | \psi^{(+)}_{\vec{p}} \rangle \quad (40)$$

and

$$S_{SC}^{(fin)} = m\int d\vec{p}'' \left\langle \psi^{(-)}_{\vec{p}'} \middle| H_{em} \middle| \psi^{(-)}_{\vec{p}} \right\rangle \frac{1}{\vec{p}^2 - \vec{p}''^2 + i\epsilon} T^{SC}_{\vec{p}'',\vec{p}}. \quad (41)$$

These terms are evaluated in the center of mass of the incoming and outgoing protons, respectively, and then boosted to the frame of interest. The matrix elements of the electromagnetic vertex are evaluated in coordinate space by first making a partial-wave expansion of the Coulomb and plane-wave functions, computing the angular integrals analytically and the radial integrals numerically. Explicit expres-

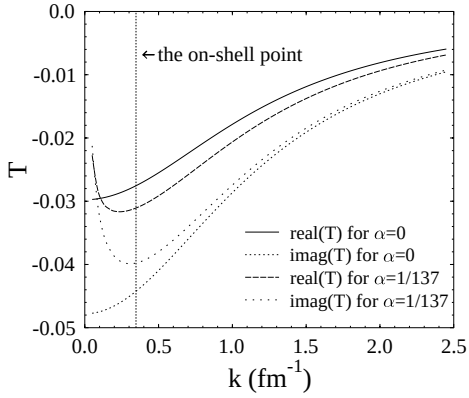

FIG. 8. The T matrix as a function of the off-shell momentum k, for the separable potential with $g(p)=1/(p^2+\beta^2)$ at a laboratory energy of 10 MeV. The curves describe a *pp* system in the presence (dashed and dotted lines) or absence (full and short-dashed lines) of the electromagnetic interaction.

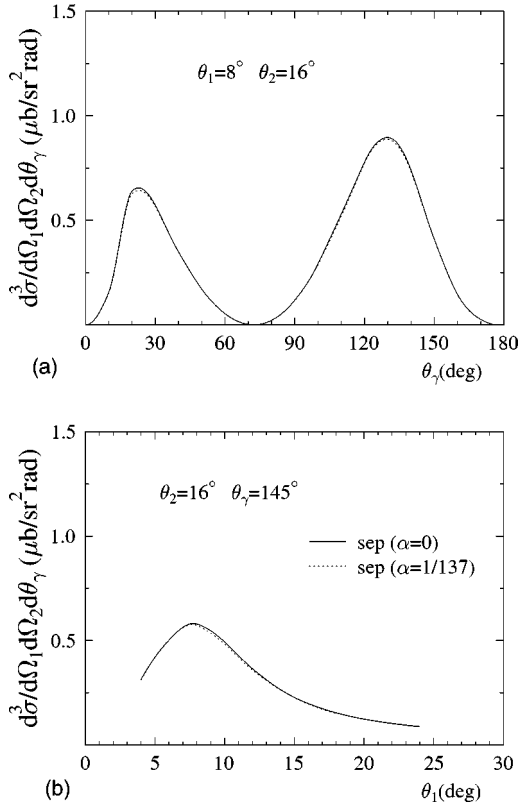

FIG. 9. Bremsstrahlung cross sections at T_{lab}=190 MeV incoming proton kinetic energy for two different kinematics: θ_2=16°,θ_γ=145° as a function of θ_1 and θ_1=8°,θ_2=16° as a function of θ_γ. The results were obtained using the toy model for bremsstrahlung described in this section. Calculations with (dotted line) and without (full line) Coulomb corrections are shown, but the two are difficult to distinguish in this plot, due to the small difference between them.

sions of the Coulomb wave functions in coordinate space can be found in Ref. [30]. Due to the fact that we deal only with a $^1S_0$ strong potential the summations over various angular momenta involved simplify considerably. Finally, the integral over the off-shell momentum is performed numerically. Checks have been performed by comparing the numerical result with the analytical result for α=0. Details of the cross-section computation formalism will be omitted; we refer to [24] for a general discussion and to [25] for the specific case of bremsstrahlung.

The influence of the Coulomb interaction on the $pp\gamma$ cross section has been studied before [8,3,31,32]. Large effects have been reported for the case of small symmetric outgoing proton angles ($\theta_1=\theta_2$) and low energy of the incoming protons [3]. This is due to the fact that for this particular case the elastic T matrix is probed at low energy, case for which the Coulomb corrections are large (Fig. 8). For energies of the projectile proton higher than 100 MeV, the effect of including the Coulomb interaction was shown to be small (of the order of a few percent), for certain kinematics with symmetric outgoing protons.

Our findings are consistent with the above mentioned results, as can be seen from Fig. 9. There we present the effect of the Coulomb interaction on the differential cross section for the two kinematics already discussed in the previous sec-

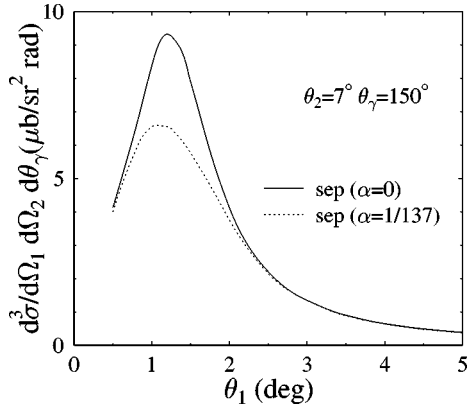

FIG. 10. Differential cross section for bremsstrahlung for variable θ_1. This particular set was chosen to illustrate the dependence of the Coulomb contribution as a function of the energy of the final protons. For the point at θ_1=1° the elastic T matrix is evaluated at an energy of 1.6 MeV for the initial-state emission diagram. The energy of the final protons is lowest for θ_1=1°.

tions. It is seen that the effect of Coulomb interaction is indeed small and it amounts to at most 1% of the total cross section. We have considered other shapes of the form factor $g(p)$ in Eq. (28) than the already mentioned one as well. Also in these cases the Coulomb corrections to the $pp\gamma$ cross section were found to be small. Furthermore, we have computed, as a check, some of the low-energy kinematics presented in Ref. [3] and found a good agreement. Coulomb corrections to the bremsstrahlung cross section can be important even for the case of a projectile proton with kinetic energy T_{lab}=190 MeV if the energy of the outgoing protons is very small. One such situation is presented in Fig. 10. The amount of the Coulomb correction varies rapidly as a function of θ_1 and can vary from 22% for θ_1=1° to less than 1% for θ_1=5°. This is due to a rapid variation of the kinetic energy of the outgoing protons as a function of θ_1: it is as low as 1.6 MeV for θ_1=1° and increases to 18 MeV for θ_1=5°. This type of kinematical region has not been probed by the KVI experiment, where the lowest value of the energy of the outgoing protons was around 10 MeV.

Coulomb effects in the higher partial waves are thought to be negligible. This is due to the fact that higher partial-wave contributions enter via terms evaluated at high energies. In the presented kinematical situations, a full calculation of the Coulomb effects (including the higher partial waves) will not reveal a bigger effect than the one already observed for the $^1S_0$ wave, which was at most 1%. We conclude that in the kinematical regions probed by the KVI experiment the Coulomb corrections are not important, excluding them as a possible source for the observed discrepancy between the model and the data.

From the expressions of the external-legs contributions to bremsstrahlung, it can be seen that the Coulomb corrections can appear in two places: the half off-shell elastic T matrix T^{SC} and the two-body operator (propagator plus the electromagnetic vertex $\langle\Psi^{(\pm)}|H_{em}|\Psi^{(\pm)}\rangle$), as can be seen from Eqs. (40) and (41). One can study in which of the two terms the Coulomb corrections are bigger. For that one can switch off, alternatively, the Coulomb corrections in the elastic T matrix

TABLE II. The origin of the Coulomb corrections can be revealed by setting $\alpha=0$ in the Coulomb-corrected elastic T matrix T^{SC} and in the two-body operator J in Eqs. (40) and (41) alternatively. Results for no Coulomb corrections at all ($\alpha=0$) and the full result ($\alpha=1/137$) are also presented.

$\theta_1\ \theta_2\ \theta_\gamma$	$\alpha=0$	$\alpha=1/137$	T^{SC} $(\alpha=0)$	J $(\alpha=0)$
1° 7° 150°	8.3665	6.5480	7.9101	6.9462
8° 16° 130°	0.8958	0.8870	0.8525	0.9323

and in the two-body operator. The results are presented in Table II for the following two kinematics: $\theta_1=1°$, $\theta_2=7°$, $\theta_\gamma=150°$ and $\theta_1=8°$, $\theta_2=16°$, $\theta_\gamma=130°$. The effects of the Coulomb corrections in the elastic T matrix [the column denoted by $J(\alpha=0)$] and in the two-body operator [the $T_{el}(\alpha=0)$ column] seem to have opposite effects: Coulomb effects in the elastic T matrix alone seem to lower the cross section for the first kinematics while it seems to increase it for the second. Coulomb effects in the two-body operator alone decrease the cross section in both cases, but much more than in the full result. One concludes that both ingredients are necessary if the Coulomb effect on bremsstrahlung is to be described accurately.

IV. SENSITIVITY OF BREMSSTRAHLUNG TO THE *NN* INTERACTION

In order to study the effect of the separable $^1S_0$ potentials on the $pp\gamma$ cross section in a realistic model we have modified the OBE model of Fleischer and Tjon. We have discarded any contribution from the negative-energy states, since when properly treated their effect on the bremsstrahlung cross section at 190 MeV is small [11,12]. Furthermore, we have only kept partial waves up to a total angular momentum $J=2$. Contributions of higher partial waves, although not explicitly shown here, are small. We have, however, replaced the $^1S_0$ partial-wave amplitude with the one given by the separable pp potential of the preceding section. The consequences of considering such a potential, for pp bremsstrahlung, are shown in Fig. 11. Calculations were performed using the Martinus *et al.* model for bremsstrahlung. This calculation adds to the results from Fig. 9, since contributions from the magnetic moment of the proton and from higher partial waves are included here as well. For the kinematics for which we have shown that the $^1S_0$ partial wave is dominant, some differences with respect to the original OBE model are observed. We conclude that an accurate description of the $^1S_0$ wave is important for an accurate description of bremsstrahlung.

We observed that the discrepancies between our model and the KVI data appear in kinematical regions where the $pp\gamma$ amplitude is dominated by contributions from the $^1S_0$ partial wave. Two possible sources for this inaccuracy were identified, the difference between a pp and a np potential in this region and Coulomb corrections to the elastic T matrix. Regarding the interference of the strong and the Coulomb interaction, we have shown in the preceding section that the difference between the pure strong bremsstrahlung and the Coulomb-modified strong bremsstrahlung is of the order of 1% at the peaks of the cross section for kinematics specific to the KVI experiment. One concludes that at least part of the discrepancy has its origin in the fact that originally the strong interaction was fitted to a potential with a scattering length $a=-23.7$ fm, which corresponds to a np system. Given the fact that for the KVI kinematics the Coulomb corrections are small, a fit of the strong interaction which would give $a=-17.1$ fm should be performed, since the OBE model does not incorporate the Coulomb interaction explicitly. Such a fit is performed by fitting the phase shifts of the model in question to the experimentally available ones. Extracting such phase shifts from the pp ones is model dependent. Lacking a model which incorporates both the Coulomb interaction and the relativistic OBE NN interaction, we have performed a fit of the relativistic OBE model of Fleischer and Tjon to the pp phase shifts of the PWA93 [33] analysis. Results using this

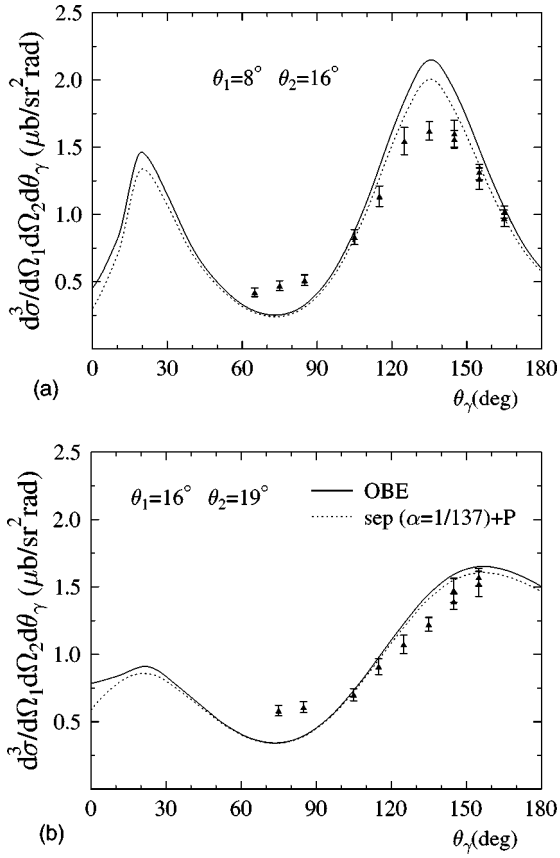

FIG. 11. Bremsstrahlung cross sections at $T_{lab}=190$ MeV incoming proton kinetic energy for two different kinematics: $\theta_1=8°, \theta_2=16°$ and $\theta_1=16°, \theta_2=19°$ as a function of θ_γ. In the OBE model the $^1S_0$ partial wave has been replaced with the one obtained from the separable potential, resulting in the dotted curve, to be compared with the original OBE result (the full line).

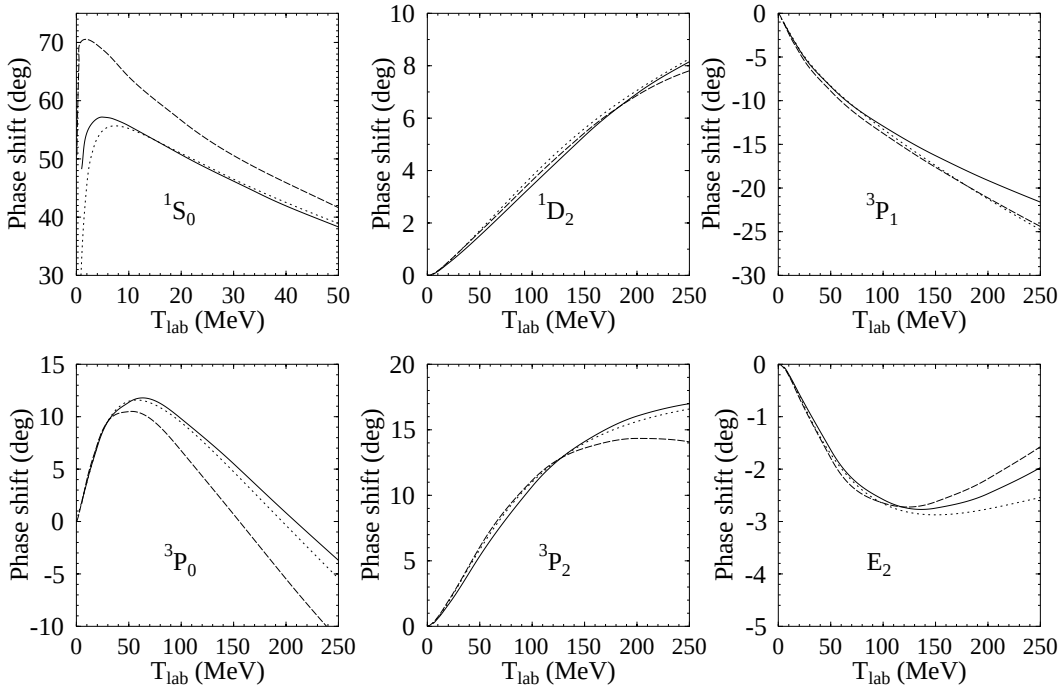

FIG. 12. A comparison between the Nijmegen PWA93 strong *pp* phase shifts (dotted line) and two "predictions" of the Fleischer-Tjon model: the old one used to obtain the result of Fig. 3 (dashed line) and the one which resulted from the refit (full line). The phase shifts (in degrees) are presented as a function of the kinetic energy in MeV in the laboratory frame of the incident proton.

refitted potential have already been presented in a previous paper [20]. The range of the fit was from 5 to 215 MeV, the lower limit has been chosen having in mind that below this energy Coulomb effects will grow in magnitude and a fit of the OBE model to reproduce Coulomb effects will be less trustworthy as the energy decreases.

In Fig. 12 we compare the *pp* strong phase shifts of the Nijmegen PWA93 and those given by the Fleischer-Tjon OBE model before and after refitting. The new coupling constants for the OBE model are presented in the Table III. For comparison, the coupling constants before the refit are also shown. Most of the partial waves have been improved by the process of refitting. One observes a substantial improvement of the $^1S_0$ phase shift, which now lies very close to the experimental strong *pp* phase shift in the 5–215 MeV range (shown only up to 50 MeV in the figure). The $^3P_0$ and $^3P_2$ also show a noticeable improvement, being now close to the experimental data also in the high-energy region. An exception to the general trend of improvement is the $^3P_1$ wave which is still off in the high-energy region. In one of the previous sections, this partial wave was seen to give an important contribution (25–30 %) to the cross section even for kinematics dominated by the $^1S_0$ wave.

A possible residual on-shell dependence has been investigated by modifying the elastic T matrix to reproduce the PWA results exactly and investigating how this modifies the bremsstrahlung cross section for various kinematics. Using the results of the PWA93 [33] analysis for the *pp* phase shifts, the Coulomb-corrected matrix elements in the partial-wave basis for each value of the total angular momentum J have been computed [34]. The partial-wave amplitudes of the OBE model have then been normalized on-shell to these experimental values (in the expression below, momenta with a hat are on-shell, while the others can also be off shell),

$$T(\hat{p},k)=T^{(\mathrm{PWA})}(\hat{p},\hat{p})\cdot\frac{T^{(\mathrm{OBE})}(\hat{p},k)}{T^{(\mathrm{OBE})}(\hat{p},\hat{p})}. \tag{42}$$

This ensures that on shell, the elastic experimental data are reproduced, while keeping the off-shell structure of the elastic T matrix as dictated by the OBE model. Again, we have produced two such modifications to the initial OBE model: in the first only the $^1S_0$ partial wave has been modified in the described way, while for the second case all partial waves were subject to this modification. Bremsstrahlung has been computed by considering only the IA graphs. Partial waves with an total angular momentum higher than 2 have also been omitted.

The results are shown in Fig. 13. The case where only the $^1S_0$ wave is modified (dotted line) hardly differs from the

TABLE III. Coupling constants of the Fleischer-Tjon OBE model of *NN* interaction before (old) and after (new) the refit.

	$g_\pi^2/4\pi$	$g_\epsilon^2/4\pi$	$g_\delta^2/4\pi$	$g_\eta^2/4\pi$	$g_\rho^{V2}/4\pi$	$g_\rho^{T2}/4\pi$	$g_\omega^2/4\pi$	Λ
Old	14.20	7.60	0.75	3.09	0.43	19.88	11.0	1.5
New	12.38	5.24	0.33	10.82	0.72	18.51	6.03	1.3

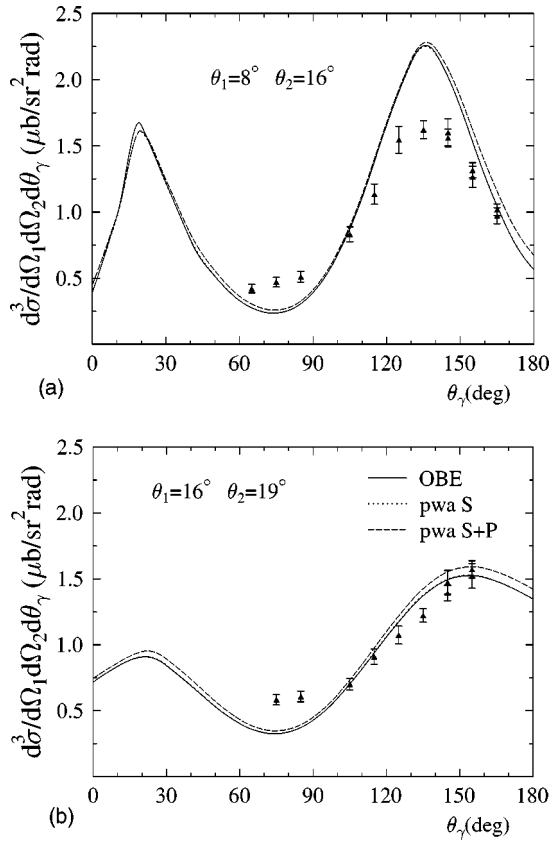

FIG. 13. Bremsstrahlung cross sections at T_{lab}=190 MeV incoming proton kinetic energy for two different kinematics: θ_1=8°,θ_2=16° and θ_1=16°,θ_2=19° as a function of θ_γ. Calculations have been performed by using the OBE model (full line) with contributions only from the positive energy states and the OBE model normalized on-shell to the PWA data (dotted and dashed lines). The full and the dotted lines fall almost on top of each other.

refitted OBE calculation, suggesting that now the low-energy behavior of the *pp* potential is properly reproduced. When all partial waves are normalized (dashed line), a slight increase in the cross section is observed for both cases presented, with a stronger increase for the *P*-wave dominated kinematics. This is due to the fact that after the refit the *P*-waves phase shifts still deviate at high energies from the experimental ones, the on-shell normalization causing the elastic *T*-matrix in these channels to increase towards the experimental data. In Table IV we have listed the various partial-wave contributions to the IA graphs both before and after the on-shell normalization has been performed. Each of the $^3P_1$ and $^3P_2$ partial-wave contributions suffer changes of the order of 10–15 %, but when all partial waves are considered together, the change is at most 5%. We conclude that after the new fit has been performed there is still a sensitivity to the on-shell *NN* interaction, which might trigger a change of at most 5% in the bremsstrahlung cross section once a perfect fit to the elastic *NN* scattering data is obtained.

To conclude, we present the cross section and analyzing power predictions for the new fit. The full $pp\gamma$ model is used, contributions from the negative-energy states and two-body currents being thus included. From Fig. 14 it is seen that the

TABLE IV. Comparison of the partial-wave contributions to the IA graphs as computed with the refitted or the on-shell normalized potential.

	$\theta_1, \theta_2, \theta_\gamma$			
	8°, 16°, 139.5°		16°, 19°, 159.3°	
	New fit	Normalized	New fit	Normalized
$^1S_0$	1.513	1.507	0.379	0.384
$^3P_0$	0.024	0.022	0.024	0.021
$^3P_1$	0.114	0.129	0.167	0.189
$^3P_2$	0.378	0.423	0.513	0.575
$^1D_0$	0.003	0.003	0.001	0.002
IA	2.207	2.242	1.514	1.584

cross-section predictions for the θ_2=16°,θ_γ=145° and θ_1=8°,θ_2=16° are improved by the new fit. A decrease of the discrepancy has been achieved by improving the low-energy part of the strong interaction, but a sizable discrepancy remains. Turning our attention to the analyzing powers, we notice that the new fit somewhat improves the predicted values with respect to the experimental data, especially for the θ_2=16°,θ_γ=145° and θ_1=16°,θ_γ=145°. The overall agreement with the experimental data remains satisfactory, also due to the fact the experimental values of this observable carry rather large error bars.

V. FINAL REMARKS

We have demonstrated the sensitivity of the bremsstrahlung observables to the low-energy *NN* interaction. The $pp\gamma$ cross section at 90 MeV varies strongly throughout the allowed phase space, the maxima corresponding to situations where the elastic *NN T* matrix is evaluated at very low energies. In the cases dominated by the $^1S_0$ partial wave, a significant discrepancy between theory and experiment has been previously observed. It was shown here that an important part of it originates in a poor description of the *NN* interaction at low energies (the $^1S_0$ channel). For the kinematics discussed here, the corrections due to the Coulomb interaction were shown to be minor. A similar conclusion was drawn for the importance of the two-body currents. The *NN* potential was improved by a refit of the Fleischer-Tjon potential to the *pp* phase shifts in the 5–215 MeV region. This resulted in an improved $^1S_0$ phase shift (especially in the low-energy region), along with other phase shifts. The analyzing powers have been improved somewhat due to the refit of the *NN* interaction, their rather good agreement with the experimental data still holding. Using the refitted potential an improvement in the description of the bremsstrahlung cross sections is observed. This improvement is mainly due to the change of the scattering length from the value of an *np* system towards the value of the *pp* system. However, a sizable discrepancy, of unclear origin, persists for the cross sections.

ACKNOWLEDGMENTS

This work was a part of the research program of the "Stichting voor Fundamenteel Onderzoek der Materie"

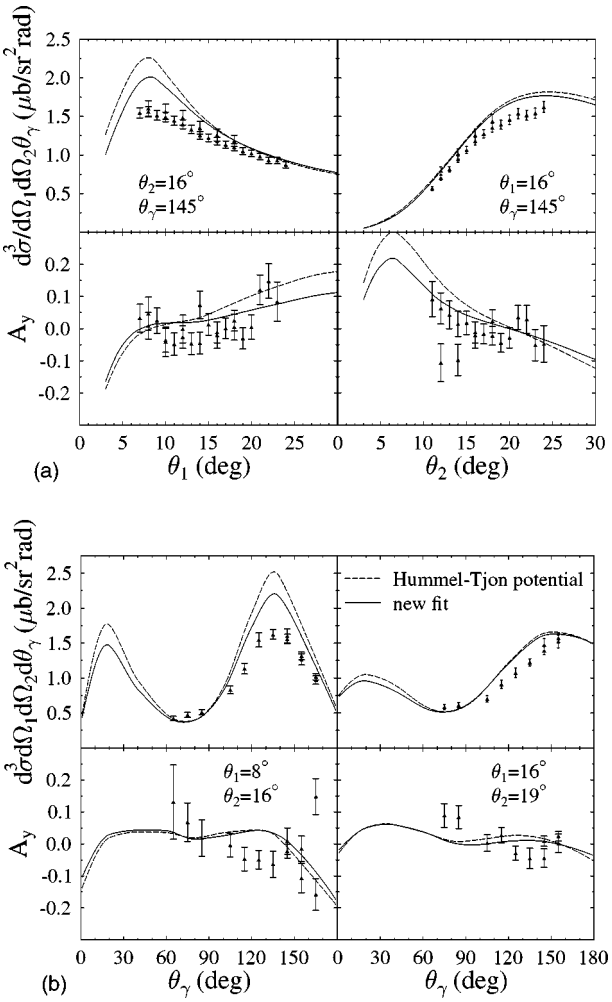

FIG. 14. Cross sections and analyzing powers for bremsstrahlung at T_{lab}=190 MeV for the four kinematics discussed in the text. Full line represents the old calculation while the dashed one represents the calculation using the new potential. Both calculation were done considering the full model of Martinus *et al.* for bremsstrahlung. As usual, the experimental data are from the KVI experiment.

(FOM) with financial support from the "Nederlandse Organisatie voor Wetenschappelijk Onderzoek" (NWO). R.G.E.T. would like to acknowledge the Royal Netherlands Academy of Arts and Sciences for financial support. This work was supported in part by the DOE Grant No. DE-FG02-93ER-40762 (J.A.T.).

APPENDIX A: TREE LEVEL POTENTIALS IN THE OBE MODEL

In the OBE model of Fleischer and Tjon contribution of the following mesons have been included: π, ρ, δ, η, ω, and ϵ. The tree level potentials of the isovector mesons π, ρ, and δ are given, respectively, by

$$V_\pi(k,p) = -ig_\pi^2[\gamma_5(\not{k}-\not{p})]^{(1)}\Delta_\pi(k-p) \times[\gamma_5(\not{k}-\not{p})]^{(2)}\vec{\tau}_1\cdot\vec{\tau}_2,$$

$$V_\rho(k,p) = -ig_\rho^V\left(\gamma_\alpha^{(1)} - \frac{ig_\rho^T}{2M}\sigma_{\alpha\mu}^{(1)}(k-p)^\mu\right)\Delta_\rho^{\alpha\beta}(k-p)\cdot\left(\gamma_\beta^{(2)} - \frac{ig_\rho^T}{2M}\sigma_{\beta\nu}^{(2)}(k-p)^\nu\right)\vec{\tau}_1\cdot\vec{\tau}_2,$$

$$V_\delta(k,p) = -ig_\delta^2\Delta_\delta(k-p)\vec{\tau}_1\cdot\vec{\tau}_2, \tag{A1}$$

and for the isoscalar mesons η, ω, and ϵ by

$$V_\eta(k,p) = -i\frac{g_\eta^2}{4M^2}[\gamma_5(\not{k}-\not{p})]^{(1)}\Delta_\eta(k-p)[\gamma_5(\not{k}-\not{p})]^{(2)},$$

$$V_\omega(k,p) = -ig_\omega^{v2}\gamma_\alpha^{(1)}\Delta_\omega^{\alpha\beta}(k-p)\gamma_\beta^{(2)},$$

$$V_\epsilon(k,p) = -ig_\varepsilon^2\Delta_\varepsilon(k-p), \tag{A2}$$

where the bracketed upper indices denote the nucleon on which operators act, $\Delta(p)$ is the propagator of scalar (δ, ϵ) and isoscalar (π, η) mesons, while $\Delta^{\mu\nu}(p)$ is the propagator of vector mesons (ρ, ω); k and p are the four-momenta of the final and the initial nucleons, respectively. To ensure the correct behavior at high momenta, a cutoff of the monopole form,

$$F(p^2) = \frac{\Lambda^2}{\Lambda^2 - p^2}, \tag{A3}$$

is introduced at each nucleon-meson vertex, with Λ being the cutoff mass. In the present OBE model the same cutoff mass is taken for each meson.

APPENDIX B: TWO-BODY CURRENT CONTRIBUTIONS

In the Martinus *et al.* model for bremsstrahlung the two-body currents have been included in a perturbative way. Besides the Born term, single- and double-scattering contributions have been considered. The current operator for contributions from meson-exchange currents (MEC) and the Δ isobar has the following expression in the center of mass of the incoming nucleons:

$$J_\mu^{MEC+\Delta} = \int\int \frac{d^4k'}{(2\pi)^4}\frac{d^4k}{(2\pi)^4}U(\Lambda)\overline{\Psi}(p',k';P')U^{-1}(\Lambda)(\Gamma_\mu^{MEC} + \Gamma_\mu^\Delta)\Psi(k,p;P), \tag{B1}$$

where Λ denotes the Lorentz transformation from the c.m. system of the final nucleons to the center-of-mass (c.m.) of the initial nucleons, Γ_μ^{MEC} and Γ_μ^Δ represent the coupling of a photon to the *NN* system via MEC or a Δ isobar, and Ψ is a two-nucleon scattering state, given for the initial nucleons by

$$\Psi(p',p;P) = [(2\pi)^4\delta^4(p'-p) - iS_2(p',P)T(p',p;P)]|p,P\rangle, \tag{B2}$$

where $|P\rangle$ is an antisymmetrized two-particle plane wave. In evaluating the four-dimensional integrals the BSLT approximation is again employed, and further, in performing the k_0 integration, only contributions from the intermedi-

ate nucleonic poles are retained.

In the case of *pp* bremsstrahlung the leading-order meson-exchange contributions, the seagull and the pion-in-flight terms vanish because in this case the exchanged particles are neutral. Therefore, the leading contributions come from decay-type diagrams [Fig. 2(a)]. The coupling of mesons to nucleons is described identically as in the OBE model. The vertex of the decay of either of the vector mesons into the pion and photon is given by

$$\Gamma^{\mu\nu}_{v\pi\gamma} = -i\frac{eg_{v\pi\gamma}}{2m_v}\epsilon^{\mu\sigma\nu\tau}q_\sigma k^v_\tau. \tag{B3}$$

The leading contributions involving the Δ isobar are also of decay type [Figs. 2(b) and 2(c)]. The $\pi N\Delta$ and $\rho N\Delta$ vertices are taken to be of the form

$$\Gamma^{\mu}_{\pi N\Delta}(k) = \frac{g_{\pi N\Delta}}{m_\pi}\Theta^{\mu\nu}(Z_\pi)k_\nu,$$

$$\Gamma^{\mu\nu}_{\rho N\Delta}(k) = i\frac{g_{\rho N\Delta}}{m_\rho}[\not{k}/k\Theta^{\mu\nu}(Z_\rho) - \gamma^\mu k_\sigma\Theta^{\alpha\nu}(Z_\rho)]\gamma_5, \tag{B4}$$

with

$$\Theta^{\mu\nu}(Z) = g^{\mu\nu} - \left(\frac{1}{2} + Z\right)\gamma^\mu\gamma^\nu, \tag{B5}$$

with $Z=1/2$ within the presented model.

[1] J. Ashkin and R. Marshak, Phys. Rev. **76**, 58 (1949); M. I. Sobel and A. H. Cromer, *ibid.* **132**, 2698 (1963); M. K. Liou and M. I. Sobel, Ann. Phys. (N.Y.) **72**, 323 (1972); D. Drechsel and L. C. Maximon, *ibid.* **49**, 403 (1968).

[2] V. R. Brown, Phys. Rev. **177**, 1498 (1969).

[3] L. Heller and M. Rich, Phys. Rev. C **10**, 479 (1974).

[4] R. L. Workman and H. W. Fearing, Phys. Rev. C **34**, 780 (1986); M. Jetter and H. W. Fearing, *ibid.* **51**, 1666 (1995).

[5] V. R. Brown, P. L. Anthony, and J. Franklin, Phys. Rev. C **44**, 1296 (1991).

[6] V. Herrmann and K. Nakayama, Phys. Rev. C **46**, 2199 (1992); F. de Jong, K. Nakayama, and T. S. H. Lee, *ibid.* **51**, 2334 (1995); F. de Jong and K. Nakayama, *ibid.* **52**, 2377 (1995).

[7] A. Katsogiannis and K. Amos, Phys. Rev. C **47**, 1376 (1993).

[8] V. Herrmann, K. Nakayama, O. Scholten, and H. Arellano, Nucl. Phys. **A582**, 568 (1994).

[9] J. A. Eden and M. F. Gari, Phys. Lett. B **347**, 187 (1995); Phys. Rev. C **53**, 1102 (1996).

[10] M. K. Liou, R. Timmermans, and B. F. Gibson, Phys. Lett. B **345**, 372 (1995); Phys. Lett. B **355**, 606(E) (1995); Phys. Rev. C **54**, 1574 (1996); R. G. E. Timmermans, B. F. Gibson, Y. Li, and M. K. Liou, *ibid.* **65**, 014001 (2001).

[11] G. H. Martinus, O. Scholten, and J. A. Tjon, Phys. Lett. B **402**, 7 (1997); Few-Body Syst. **26**, 197 (1999); G. H. Martinus, Ph.D. thesis, University of Groningen, 1998.

[12] G. H. Martinus, O. Scholten, and J. A. Tjon, Phys. Rev. C **56**, 2945 (1997).

[13] A. Yu. Korchin, O. Scholten, and D. van Neck, Nucl. Phys. **A602**, 423 (1996); A. Yu. Korchin, O. Scholten, and F. de Jong, Phys. Lett. B **402**, 1 (1997); S. Kondratyuk, G. H. Martinus, and O. Scholten, *ibid.* **418**, 20 (1998).

[14] K. Michaelian *et al.*, Phys. Rev. D **41**, 2689 (1990).

[15] H. Huisman *et al.*, Phys. Rev. Lett. **83**, 4017 (1999); Phys. Lett. B **476**, 9 (2000); H. Huisman, Ph.D. thesis, University of Groningen, 1999.

[16] J. Fleischer and J. A. Tjon, Nucl. Phys. **B84**, 375 (1974); Phys. Rev. D **15**, 2537 (1977); J. Fleischer and J. A. Tjon, *ibid.* **21**, 87 (1980).

[17] A. Logunov and A. Tavkhelidze, Nuovo Cimento **29**, 380 (1963); R. Blankenbecler and R. Sugar, Phys. Rev. **142**, 1051 (1966).

[18] E. Hummel and J. A. Tjon, Phys. Rev. C **42**, 423 (1990); Phys. Rev. C **49**, 21 (1994); Phys. Rev. Lett. **63**, 1788 (1989); E. Hummel, Ph.D. thesis, University of Utrecht, 1991.

[19] R. A. Arndt, J. S. Hyslop, III, and L. D. Roper, Phys. Rev. D **35**, 128 (1987).

[20] M. D. Cozma, G. H. Martinus, O. Scholten, R. G. E. Timmermans, and J. A. Tjon, Phys. Rev. C **65**, 024001 (2002).

[21] F. E. Low, Phys. Rev. **110**, 974 (1958).

[22] H. Huisman *et al.*, Phys. Rev. C **65**, 031001 (2002).

[23] M. Gell-Mann and M. L. Goldberger, Phys. Rev. **91**, 398 (1953).

[24] M. L. Goldberger and K. M. Watson, *Collision Theory* (Wiley, New York, 1964).

[25] D. Drechsel and L. C. Maximon, Ann. Phys. (N.Y.) **49**, 403 (1968).

[26] D. J. Ernst, C. M. Shakin, and R. M. Thaler, Phys. Rev. C **8**, 46 (1973); Phys. Rev. C **9**, 1780 (1974).

[27] J. Haidenbauer and W. Plessas, Phys. Rev. C **30**, 1822 (1984); Phys. Rev. C **32**, 1424 (1985).

[28] G. E. Brown and A. D. Jackson, *The Nucleon-Nucleon Interaction* (North-Holland, Amsterdam, 1976).

[29] D. R. Harrington, Phys. Rev. **139**, B691 (1967).

[30] L. D. Landau and E. M. Lifshitz, *Quantum Mechanics: Non-relativistic Theory* (Pergamon, New York, 1977).

[31] A. Katsogiannis, K. Amos, M. Jetter, and H. V. von Geramb, Phys. Rev. C **49**, 2342 (1994).

[32] T. D. Penninga and R. G. E. Timmermans, KVI report 2001.

[33] See the NN-OnLine database, http://nn-online.sci.kun.nl; V. G. J. Stoks, R. A. M. Klomp, M. C. M. Rentmeester, and J. J. de Swart, Phys. Rev. C **48**, 792 (1993); M. C. M. Rentmeester, R. G. E. Timmermans, J. L. Friar, and J. J. de Swart, Phys. Rev. Lett. **82**, 4992 (1999)

[34] N. Hoshizaki, Suppl. Prog. Theor. Phys. **42**, 107 (1968).